Asad, Bilal; Vaimann, Toomas; Kallaste, Ants; Belahcen, Anouar

Harmonic spectrum analysis of induction motor with broken rotor bar fault

Published in:
Proceedings of the 2018 IEEE 59th Annual International Scientific Conference on Power and Electrical Engineering of Riga Technical University, RTUCON 2018

DOI:
10.1109/RTUCON.2018.8659842

Published: 04/03/2019

Document Version
Peer-reviewed accepted author manuscript, also known as Final accepted manuscript or Post-print

Please cite the original version:
Asad, B., Vaimann, T., Kallaste, A., & Belahcen, A. (2019). Harmonic spectrum analysis of induction motor with broken rotor bar fault. In *Proceedings of the 2018 IEEE 59th Annual International Scientific Conference on Power and Electrical Engineering of Riga Technical University, RTUCON 2018* Article 8659842 IEEE. https://doi.org/10.1109/RTUCON.2018.8659842

Harmonic Spectrum Analysis of Induction Motor With Broken Rotor Bar Fault

Bilal Asad, Toomas Vaimann, Ants Kallaste
Dept. of Electrical Power Engineering and Mechatronics
Tallinn University of Technology
Tallinn, Estonia
biasad@ttu.ee

Anouar Belahcen
Dept. of Electrical Engineering and Automation
Aalto University
Espoo, Finland

***Abstract*—In this paper, the frequency spectrum of a three-phase induction motor's stator current on a linear scale is investigated. The broken rotor bar, spatial and grid fed harmonics are taken into consideration. Since the fundamental component of the power supply is always the most powerful component, it makes the spectrum less legible, increases the spectral leakage and makes the logarithmic scale inevitable. In this paper, a Chebyshev filter is used for attenuation of the fundamental component, because of its good transition band and no passband ripples. The current signals are taken from both simulation and laboratory environment and harmonics due to above-mentioned causes are segregated.**

Keywords— digital filters; fault diagnosis; induction motors; Fourier transform.

I. INTRODUCTION

From the starting of the second industrial revolution, induction motor has become a key element of modern day industry because of its variety of applications, ranging from generation to consumer domains. In the form of doubly fed induction generators, they are an integral part of renewable energy resources, such as wind power plants, and in the form electrical to mechanical energy converters, they are driving the cycle of industry, making an impact on a nation's economy. They are also being extensively used in commercial and domestic applications, such as electric vehicles, fans, water pumps, etc. There are many machines which can convert electrical energy to mechanical energy, but inductions motor's simple structure, good efficiency and easy repair have made them the most common among all. They are the biggest consumer of electricity, consuming about 50% of total generated energy worldwide [1].

These machines remain always vulnerable to faults because of mechanically moving parts associated with it. These faults can be broadly classified into electrical and mechanical categories. Electrical faults are mainly associated with stator such as voltage imbalance, phase drop, inter-turn short circuits and earthing faults, etc. Mechanical faults make the biggest proportion of overall faults, such as damaged bearings, broken rotor bars, broken end rings and eccentricity faults, etc.

These faults are directly or indirectly related with each other and are degenerative in nature. Hence, it is very important to detect them at an incipient stage in order to avoid extensive economic loss and time-consuming repair processes.

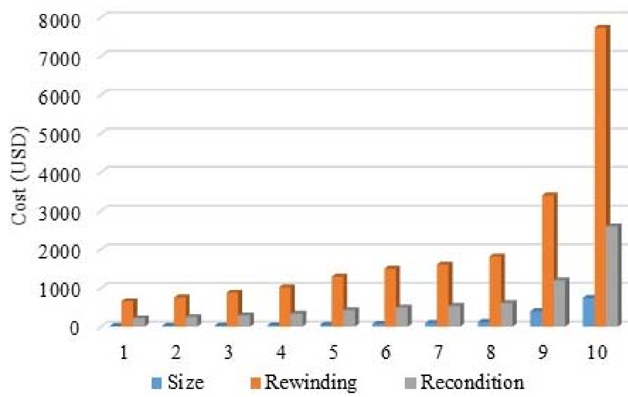

Fig. 1. Recondition vs rewind cost of different power induction motors.

Fig. 1 shows a comparative difference between recondition and rewind cost of different power induction motors as proposed by Penrose in [2]. Due to the above mentioned facts, the field of fault diagnostics becomes to be as important as the field of machine design and control.

Motor current signature analysis (MCSA) based fault diagnostic techniques are being extensively used in research, because these techniques are mostly noninvasive in nature and require simple measurements. After the current measurement, there comes an entire domain of signal processing techniques to estimate the nature and the severity of the fault.

Fourier series has led the foundation of almost all kind of modern signal processing techniques. The majority of signal processing-based fault diagnostic techniques depend on Fourier analysis because of the need to investigate the frequency spectrum. This is so, because every kind of fault leaves some specific harmonics in the frequency spectrum of the stator current. The majority of MCSA based techniques depend on fast Fourier transform (FFT) of the signal, e.g. in [3], the authors used the FFT on active and reactive currents of a motor to investigate the broken rotor bars and load oscillations. Authors of [4] used the FFT in conjunction with Park's vector to make artificial ants clustering technique for the fault diagnostics of induction motor. In [5], the autoregressive method is relying on discrete time Fourier transform (DTFT) and notch filter. Researchers in [6] used the FFT to prove that the slot harmonics can be used as potential indicators to detect the broken rotor bars. In [7], the authors used an adoptive notch filter and FFT for broken rotor bar fault diagnostics of induction motor. Authors of [8] used the FFT on simulations and practical results to investigate the broken rotor bars and mechanical vibrations. In [9], Nandi used the FFT extensively to study the frequency spectrum of the stator current for different fault conditions.

The most profound problem with the FFT is the spectral leakage of the fundamental component. The fundamental component contains more power as the other higher order harmonics, such as the spatial and the fault baring harmonics. Therefore, the logarithmic scale is usually preferred for better legibility of the spectrum, but spectral leakage remains and is likely to hide the frequency components near the fundamental component. In addition, at low slip conditions, spectral leakage problem becomes severe, because in case of most of the rotor-associated faults, the frequencies depend on the slip. Some techniques can be found in literature, in which the researchers have tried to reduce the problem of the spectral leakage. Authors of [10] have used the Hilbert transform to get the envelope of the signal, containing potential information about the faults.

In this paper, the Chebyshev filter is used for its better brick wall characteristics compared to other filters, such as Butterworth, Hilbert, etc. Unlike most of the papers, which focus mainly on the frequency spectrum containing faulty frequency harmonics on the logarithmic scale, while neglecting the supply fed harmonics, in this paper the entire frequency spectrum on linear scale is studied, using the motor currents taken from both finite element-based simulations and experiments. Moreover, the grid fed harmonics are also tracked to make the picture clearer. It is shown that the proposed filter makes the spectrum much more legible and removes the fundamental component effectively without disturbing all other harmonics.

II. Mathematical Background

A. Slots and Broken Bar Harmonics

In case of a healthy motor, the frequency spectrum of the stator and rotor current contains a number of harmonics, because of the distributed nature of rotor and stator windings, even if the supply is taken as ideal. These harmonics can be represented with the help of stator current linkage and the winding factor by the following equation [1]:

$$MMF\ (t,\alpha) = \frac{3}{\pi}\left(\frac{k_{wf}N_s}{vp}\right)\left(Ie^{\ j(\omega t - v\alpha)}\right), \tag{1}$$

$$k_{wf} = \frac{sin\frac{n\pi}{2}}{N}\sum_{\rho=1}^{N}\cos\propto_p, \tag{2}$$

where N_s is the number of conductors per phase, k_{wf} is the winding factor, p is the number of pole pairs, v is the harmonic number, N is the total number of slots and α is the angle of the corresponding slot.

Every fault modulates the stator current with a specific frequency and modulation index, depending upon the severity of the fault. These fault frequencies can be described mathematically as a function of rotor and stator geometrical and electrical parameters. Extensive mathematics representing these faults can be found in [9], [11]-[14] and the simplified version in [15]. The detection of broken bar at an incipient stage is necessary, because when one bar breaks, its consecutive bars come under more thermal stress leading to their breakage. These faults produce the following harmonics in the frequency spectrum [16]:

$$f_{BR} = f_s \pm 2ksf_s \tag{3}$$

$$f_{BR} = [\left(\frac{k}{p}\right)(1 - \mathrm{s}) \pm \mathrm{s}]\, f_s \tag{4}$$

where k = 1,2,3,…., f_s is the supply frequency, p is the number of pole pairs and s is the slip of the machine. The lower sideband appears due to the broken rotor bar and the upper sideband due to the resultant speed oscillations. The dependency of these harmonic frequencies on the slip make them more likely to be buried under the spectrum of the fundamental component. This problem becomes the worst under small and no-load conditions. In addition, the amplitude of these frequencies depends on the number of broken bars and is relatively small compared to the amplitude of the supply frequency

B. Fourier Transform

The FFT is being used in almost every field of science, as it yields the possibility to segregate a non-periodic random signal into sinusoids, having specific frequency and amplitude, called the harmonics. The amplitude of these harmonics usually attenuates as they travel along the frequency axis, making the fundamental component the most significant one. The discrete Fourier transform (DFT) and its inverse can be represented by the following formulas:

$$X_k = \sum_{n=0}^{N-1} x_n\, e^{-i2\pi kn/N}, \quad k = 0,1,2,\dots,(N-1), \tag{5}$$

$$x_n = \frac{1}{N}\sum_{n=0}^{N-1} X_n\, e^{-i2\pi kn/N}, \quad k = 0,1,2,\dots,(N-1), \tag{6}$$

where N is the number of samples, n is the current sample, x_n is the value of the signal at time n, k is the current frequency and X_k is the resultant bin of DFT. For a complete and accurate frequency spectrum, frequency resolution is very important, which depends upon the measurement time of the signal and the sampling frequency, as shown in the following equation:

$$\Delta f = {}^{1}/_{T_m} = {}^{f_s}/_{N} = {}^{BW}/_{SL} = {}^{2 * BW}/_{N}, \tag{7}$$

where Δf is the frequency difference between two consecutive frequency bins, N is the number of samples, BW is the bandwidth and SL is the number of spectral lines.

Since the taken signal is of a finite length and the length of the signal may not be an integer multiple of all frequency components, this will lead to a problem of spectral leakage. Being the most significant component, fundamental component can have a larger tendency of spectral leakage, amplifying the need of an attenuation filter.

C. Chebyshev Filters

Digital filters are mathematical algorithms, which are capable to reduce or enhance certain parameters of a signal. Because of their diversified nature, they have many types and are being used extensively in almost every signal processing-based application.

Chebyshev filters are well known for their better step response as compared to the Butterworth filter. Its gain response as a function of frequency ω can be represented as:

$$G_n(\omega) = 1/\sqrt{1 + \varepsilon^2 T_n^2(\omega / \omega_o)} \tag{8}$$

Where ε is ripple factor, ω_o is cutoff frequency and T_n is its polynomial of nth order.

Fig. 2 shows a comparative analysis of Butterworth and Chebyshev type I and type II filters for the same tuning parameters. It is evident that the Butterworth filter is flat in its passband interval but has a bad roll-off, which can be fatal for fault frequencies lying very close to the fundamental component in case of a broken rotor bar. Chebyshev filters have a very good transition band but have ripples in the passband in case of type I, and stopband in case of type II.

Fig. 2. Step response of Butterworth and Chebyshev filters.

D. *Finite Element Method for Motor Simulation*

The mathematical modeling and simulations of induction motors are extremely important, as it is a fundamental milestone for design and control procedures. The more accurate the mathematical model of the machine is, the more accurate its practical design and control would be. The most common

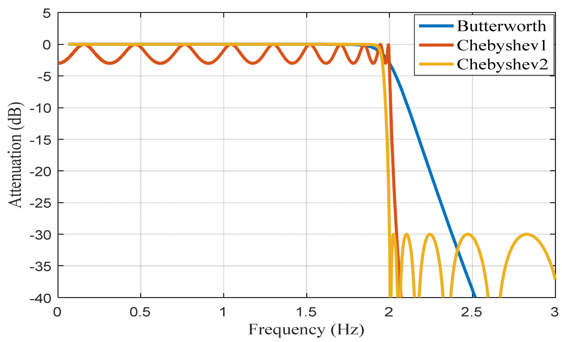

method of modeling found in literature, is the analytical method, in which the system is described with the help of integro-differential equations. Analytical models usually neglect the complex nonlinear behavior of the system to make it more simple. With the increase in computational power, the numerical models such as FEM are gaining more and more popularity in the field of modeling and simulations. These models are good approximations of an actual system, as they consider all possible parameters, but at the cost of complexity and long computational time. The numerical model of induction motor relies on the Maxwell's equations:

$$\nabla \times E = -\frac{\partial B}{\partial t} \tag{9}$$

$$\nabla \times H = J + \frac{\partial D}{\partial t} \tag{10}$$

$$H = \nu B \tag{11}$$

$$J = \sigma E \tag{12}$$

Where E is the electric field strength, B is the magnetic flux density, D is displacement current, D is electric flux density, H is the magnetic field strength, J is the current density, ν is the magnetic reluctivity of material and σ is its electric conductivity.

By assuming that the magnetic field lies in an x-y plane, varies sinusoidally in time and induces currents in the z-direction, the vector potential A distributes in the machine according to the following equation [17]:

$$\frac{\partial}{\partial x}\left(\frac{1}{\mu}\right)\frac{\partial A}{\partial x} + \frac{\partial}{\partial y}\left(\frac{1}{\mu}\right)\frac{\partial A}{\partial y} - s\frac{\partial}{\partial t}(\sigma A) + J = 0 \tag{13}$$

If the conductivity of the rotor and stator laminations is taken as zero, and the reluctivity of conducting regions as that of the vacuum, the electric scalar potential and voltage equation of a conductor can be represented as [8]:

$$\nabla \varphi = -\frac{u}{l} e_z, \tag{14}$$

$$u = iR + R \oint \sigma \frac{\partial A_z}{\partial t} .ds \tag{15}$$

III. Simulation Results and Discussion

The FEM-based simulation of a three-phase induction motor with the parameters shown in Table I is performed under healthy, one, and two broken rotor bar conditions. Since the simulation is performed using 2D field analysis, the ignored end windings are compensated by adding additional resistances and inductances in series with coils. The per phase stator coils are series and parallel connections of copper strands making current density uniformly distributed. The simulation is performed at rated load under constant speed. The flux distribution under healthy and two broken rotor bar conditions is shown in Fig. 3. It is evident that the flux density increases across broken bars, putting the adjacent bars under increased magnetic stress. The increase in the current of the neighboring bars makes the machine vulnerable to break more bars in time, if the fault is not timely diagnosed and repaired.

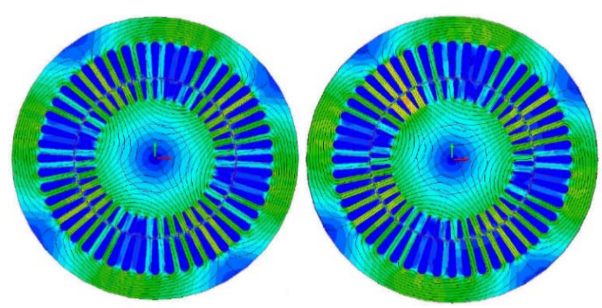

Fig. 3. Normalized magnetic field density of healthy and broken rotor bar motors.

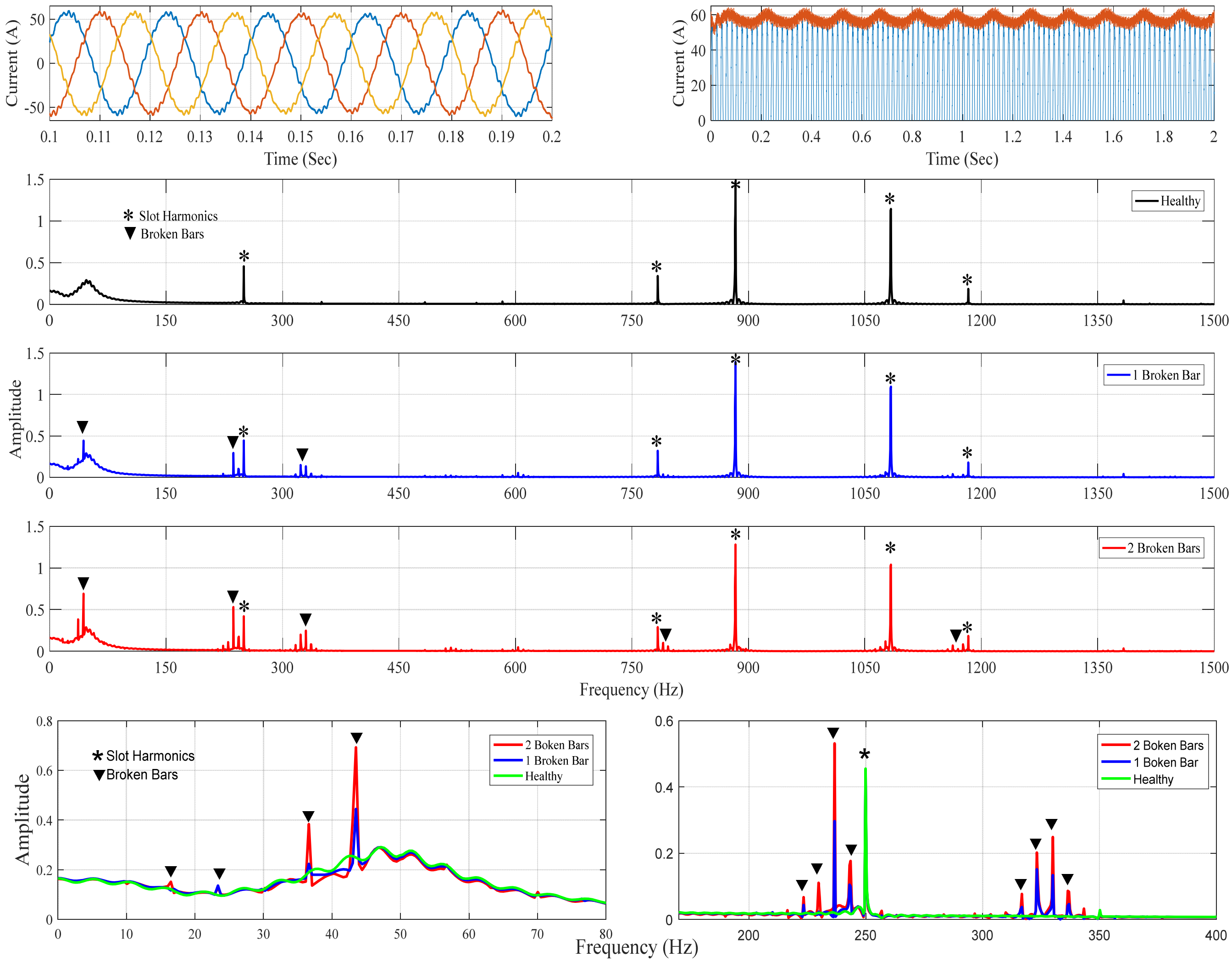

Fig. 4. Simulation results; three phase current in top left, per phase current and its envelope for three broken bars in top right, frequency spectrum for healthy, 1 broken and 2 broken bar cases from top to down; zoomed comparison of harmonics for healthy and faulty motors in bottom two graphs.

Fig. 4 shows the motor simulation results for stator currents and frequency spectrum under healthy and broken rotor bar conditions from top to bottom. In the first graph, zoomed stator current is shown, which is calculated using a step size of 0.033 ms at the rated load condition, using FEM. The simulation is performed for two seconds with 5328 mesh elements at stator and rotor temperatures of 120°C and 140°C respectively. The current seems distorted because of time and slot harmonics. The second graph is representing the positive side of the current and its envelope under two broken bar condition. The envelope is clearly representing the effect of the broken rotor bars and the modulation of the motor current. The ripples in the envelope of the current increases with the increase in the modulation index, which depends upon the number of broken bars. The distribution of the harmonics in the frequency spectrum of the stator current is shown in next three graphs for healthy, one broken bar, and two broken bar cases respectively. The fundamental component of the supply voltage is attenuated, making the spectrum legible on the linear axis. The frequency components can be easily differentiated due to the spatial and broken rotor bar harmonics. In the last two graphs, the frequency spectrums in the range of 0-80 Hz and 170-400 Hz are plotted on the same window for healthy and faulty cases, to give a comparative analysis. It is clear that the faulty frequencies are increasing in amplitude with the increase in the number of broken bars.

IV. Experimental Setup

The measurement setup consists of two same type motors with the parameters shown in Table 1. One machine is under investigation and the other one is acting as load. Both machines are mounted on the same mechanical base and coupled through their shafts as shown in Fig. 5(a). The loading machine is fed through the inverters to improve its controllability for various load levels and the machine under investigation is fed by grid supply containing some harmonics as discussed in results section. The stator currents and voltages are measured using the Dewetron transient recorder. The sampling frequency of the measured signals is 10000 samples per second and the measurement time is 70 seconds, giving a very good resolution of the frequency spectrum. Fig. 5(b) shows the block diagram of the test setup.

TABLE I. MOTOR PARAMETERS

Parameter	Symbol	Value
Number of poles	P	4
Number of phases	φ	3
Connection	Y-Δ	Star
Stator slots	N_s	48; non-skewed
Rotor slots	N_r	40; non-skewed
Terminal voltage	V	333V@50 Hz
Rated slip	S	0.0667
Rated power	P_r	18 kW@50 Hz

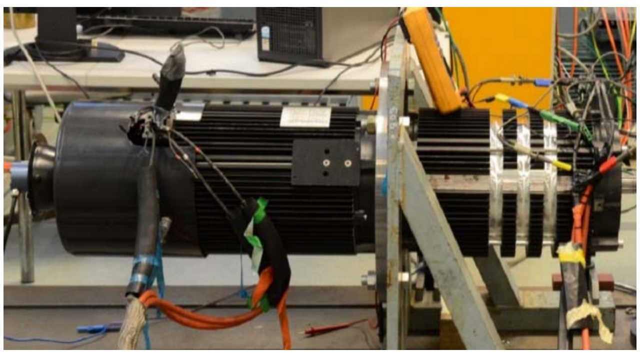

(a)

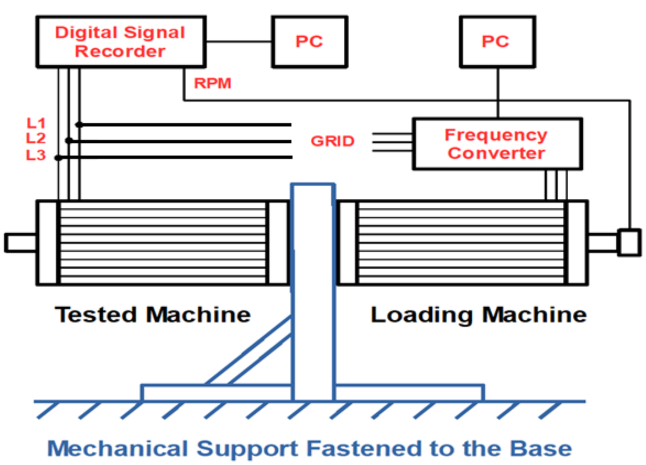

(b)

Fig. 5. (a) Experimental setup; (b) Schematic of the experimental setup.

V. RESULTS AND DISCUSSION

Fig. 6 shows the cycles of the input phase voltage and the corresponding spectrum. For a better visibility of the grid fed harmonics, the fundamental component is attenuated using the proposed filter which removes the it effectively without having any influence on the rest of the harmonics. The supply harmonics are mainly odd harmonics and can be represented by the following equation:

$$f_{SH} = kf_s\,, \qquad k = 1,3,5,\ldots \tag{16}$$

Fig. 7 presents the experimental results. The top two graphs are the stator three-phase and single-phase currents. The envelope of current is also represented using Hilbert transform to show the impact of broken rotor bars. The current is smoother than the current taken from simulation, because the skewness of rotor bars has suppressed the slot harmonics considerably. The next graphs are the frequency spectra for healthy, one, two, and three broken bars respectively. The fundamental component has been attenuated successfully, making the harmonics discoverable without using the logarithmic scale. It is evident in the results that under healthy condition the only prominent harmonics are supply harmonics, which will be many in case of inverter fed machines. These harmonics can be a misleading factor in diagnostic algorithms if not addressed properly. The last two graphs are giving a comparative analysis of all four cases on the same window, where it can be seen that the amplitude of the fault harmonics is increasing with the increase in the number of broken bars.

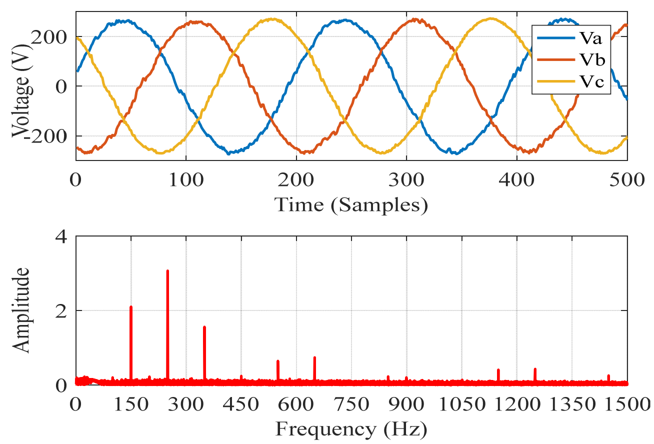

Fig. 6. Grid fed voltage and respective frequency spectrum

VI. CONCLUSIONS

The MCSA is the most common technique used for the fault diagnostics of induction motors, because of its simplicity and noninvasive nature. In this paper, harmonic spectrum of an induction motor for healthy and broken rotor bar cases using signals from the simulation and experiments is studied.

FEM.based simulations reveal that the rotor bars next to the broken one, come under more magnetic and thermal stresses making them vulnerable to break, increasing the severity of fault with the passage of time. Hence it is very important for diagnostic algorithm to be able to detect fault at incipient stage. Hence accurate attenuation of the fundamental component can lead to very accurate results.

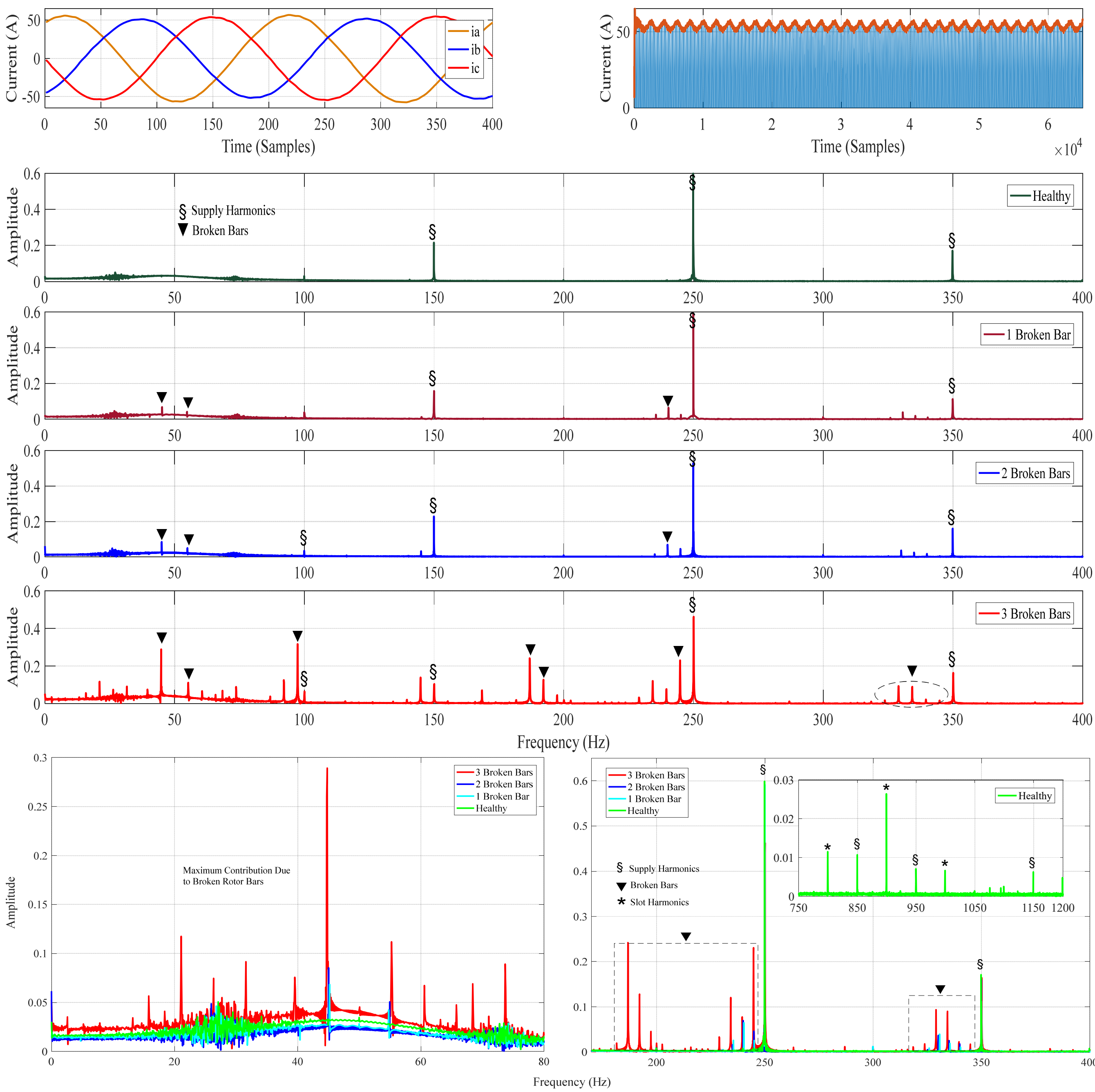

Fig. 7. Experimenta results: three phase current in top left, per phase current and its envelope for three broken bars in top right, frequency spectrum for health, one, two, and three broken bars cases from top to down; zoomed comparison of harmonics for healthy and faulty motors in the bottom.

The use of the Chebyshev filter for the attenuation of the fundamental component reduces its spectral leakage considerably. This filter has a good transition band and makes less impact on the upper and lower sidebands of the broken rotor bar frequencies. Also the less pass band ripples in case of type II filter reduces the impact of filter on frequency spectrum.

Since the most powerful component is filtered out, it improves the legibility of the spectrum even at the linear scale. From the simulation results, the broken rotor bar and high frequency slot harmonics are easily readable on the same graph. In case of the experimental setup, since the load motor is supplied from an inverter, hence the slip of test motor is carefully controlled the investigate the location of fault frequencies.

The supply harmonics should be treated carefully particularly in case of inverter fed machines in order to avoid false fault indications. It can be noticed that the slot harmonics are considerably suppressed by the skewing factor of rotor.

REFERENCES

[1] J. Pyrhönen, T. Jokinen, and V. Hrabovcová, Design of rotating electrical machines. John Wiley & Sons, 2008, p. 47-152.

[2] H. W. Penrose, "Test Methods for Determining the Impact of Motor Condition on Motor Efficiency and Reliability," PhD Diss., USA: ALL-TEST P, no. LLC, Old Saybrook, CT, pp. 1–8, March 2007.

[3] G. R. Bossio, C. H. De Angelo, J. M. Bossio, C. M. Pezzani, and G. O. Garcia, "Separating Broken Rotor Bars and Load Oscillations on IM Fault Diagnosis Through the Instantaneous Active and Reactive Currents," IEEE Trans. Ind. Electron., vol. 56, no. 11, pp. 4571–4580, Nov. 2009.

[4] A. Soualhi, G. Clerc, and H. Razik, "Detection and Diagnosis of Faults in Induction Motor Using an Improved Artificial Ant Clustering Technique," IEEE Trans. Ind. Electron., vol. 60, no. 9, pp. 4053–4062, Sep. 2013.

[5] B. Ayhan, H. J. Trussell, Mo-Yuen Chow, and Myung-Hyun Song, "On the Use of a Lower Sampling Rate for Broken Rotor Bar Detection With DTFT and AR-Based Spectrum Methods," IEEE Trans. Ind. Electron., vol. 55, no. 3, pp. 1421–1434, Mar. 2008.

[6] A. Khezzar, M. Y. Kaikaa, M. El Kamel Oumaamar, M. Boucherma, and H. Razik, "On the Use of Slot Harmonics as a Potential Indicator of Rotor Bar Breakage in the Induction Machine," IEEE Trans. Ind. Electron., vol. 56, no. 11, pp. 4592–4605, Nov. 2009.

[7] M. Malekpour, B. T. Phung, and E. Ambikairajah, "Stator current envelope extraction for analysis of broken rotor bar in induction motors," in 2017 IEEE 11th International Symposium on Diagnostics for Electrical Machines, Power Electronics and Drives (SDEMPED), 2017, pp. 240–246.

[8] A. Belahcen, J. Martinez, and T. Vaimann, "Comprehensive computations of the response of faulty cage induction machines," in 2014 International Conference on Electrical Machines (ICEM), 2014, pp. 1510–1515.

[9] S. Nandi, H. A. Toliyat, and X. Li, "Condition Monitoring and Fault Diagnosis of Electrical Motors—A Review," IEEE Trans. Energy Convers., vol. 20, no. 4, pp. 719–729, Dec. 2005.

[10] R. Puche-Panadero, M. Pineda-Sanchez, M. Riera-Guasp, J. Roger-Folch, E. Hurtado-Perez, and J. Perez-Cruz, "Improved Resolution of the MCSA Method Via Hilbert Transform, Enabling the Diagnosis of Rotor Asymmetries at Very Low Slip," IEEE Trans. Energy Convers., vol. 24, no. 1, pp. 52–59, Mar. 2009.

[11] J. R. Cameron, W. T. Thomson, and A. B. Dow, "Vibration and current monitoring for detecting airgap eccentricity in large induction motors," IEE Proc. B Electr. Power Appl., vol. 133, no. 3, p. 155, 1986.

[12] R. R. Schoen and T. G. Habetler, "Effects of time-varying loads on rotor fault detection in induction machines," IEEE Trans. Ind. Appl., vol. 31, no. 4, pp. 900–906, 1995.

[13] R. Ong, J. H. Dymond, and R. D. Findlay, "Bearing damage analysis in a large oil-ring-lubricated induction machine," IEEE Trans. Ind. Electron., vol. 47, no. 5, pp. 1085–1091, 2000.

[14] H. Henao, C. Demian, and G.-A. Capolino, "A frequency-domain detection of stator winding faults in induction machines using an external flux sensor," IEEE Trans. Ind. Appl., vol. 39, no. 5, pp. 1272–1279, Sep. 2003.

[15] A. Sapena-Bano, J. Burriel-Valencia, M. Pineda-Sanchez, R. Puche-Panadero, and M. Riera-Guasp, "The Harmonic Order Tracking Analysis Method for the Fault Diagnosis in Induction Motors Under Time-Varying Conditions," IEEE Trans. Energy Convers., vol. 32, no. 1, pp. 244–256, Mar. 2017.

[16] J. Milimonfared, H. M. Kelk, S. Nandi, A. D. Minassians, and H. A. Toliyat, "A novel approach for broken-rotor-bar detection in cage induction motors," IEEE Trans. Ind. Appl., vol. 35, no. 5, pp. 1000–1006, 1999.

[17] N. M. Elkasabgy, A. R. Eastham, and G. E. Dawson, "Detection of broken bars in the cage rotor on an induction machine," IEEE Trans. Ind. Appl., vol. 28, no. 1, pp. 165–171, 1992.

BIOGRAPHIES

Bilal Asad was born in 1986 in Pakistan. He received his BSc in Electronics Engineering from The Islamia University of Bahawalpur and MSc in Electrical Engineering from University of Engineering and Technology (UET) Lahore, Pakistan in 2007 and 2011 respectively. Currently he is a PhD student in the Department of Electrical Power Engineering and Mechatronics, Tallinn University of Technology, Estonia.
His area of interest includes design, simulations and fault diagnostics of electrical machines.

Toomas Vaimann (S'11-M'14) was born in Pärnu, Estonia, in 1984. He received his BSc, MSc and PhD degrees in Electrical Engineering from Tallinn University of Technology, Estonia in 2007, 2009 and 2014 respectively. He is currently a senior researcher in Tallinn University of Technology, Department of Electrical Power Engineering and Mechatronics.
He has been working in several companies as electrical engineer. He is member of IEEE, Estonian society of Moritz Hermann Jacobi and Estonian Society of Electrical Power Engineering.

Anouar Belahcen (M'13-SM'15) was born in Essaouira, Morocco, in 1963. He received the BSc degree in physics from the University Sidi Mohamed Ben Abdellah Fes, Moroco, in 1988 and the MSc (Tech.) and Doctor (Tech.) degrees from Helsinki University of Technology, Finland, in 1998 and 2004 respectively.
From 2008 to 2013, he has been working as Adjunct Professor in the field of coupled problems and material modeling at Aalto University, Finland. Since 2011 he is Professor of electrical machines at Tallinn University of Technology, Estonia and in 2013 he became Professor of Energy and Power at Aalto University.
His research interests are numerical modeling of electrical machines, especially magnetic material modeling, coupled magnetic and mechanical problems, magnetic forces and magnetostriction

Ants Kallaste (M'13) was born in Pärnu, Estonia, in 1980. He received his BSc, MSc and PhD degrees in Electrical Engineering from Tallinn University of Technology, Estonia in 2004, 2006 and 2013 respectively. He is currently a senior researcher in Tallinn University of Technology, Department of Electrical Power Engineering and Mechatronics.
He has been working in several companies as electrical engineer. His main research interests include permanent magnet machine design and wind turbines.